

Droplet under confinement: Competition and coexistence with soliton bound state

Xiaoling Cui^{1,2,*} and Yinfeng Ma^{1,3}

¹Beijing National Laboratory for Condensed Matter Physics,

Institute of Physics, Chinese Academy of Sciences, Beijing 100190, China

²Songshan Lake Materials Laboratory, Dongguan, Guangdong 523808, China

³School of Physical Sciences, University of Chinese Academy of Sciences, Beijing 100049, China

(Dated: October 22, 2020)

We study the stability of quantum droplet and its associated phase transitions in ultracold Bose-Bose mixtures uniformly confined in quasi-two-dimension. We show that the confinement-induced boundary effect can be significant when increasing the atom number or reducing the confinement length, which destabilizes the quantum droplet towards the formation of a soliton bound state. In particular, as increasing the atom number we find the reentrance of soliton ground state, while the droplet is stabilized only within a finite number window that sensitively depends on the confinement length. Near the droplet-soliton transitions, they can coexist with each other as two local minima in the energy landscape. Take the two-species ³⁹K bosons for instance, we have mapped out the phase diagram for droplet-soliton transition and coexistence in terms of atom number and confinement length. The revealed intriguing competition between quantum droplet and soliton under confinement can be readily probed in current cold atoms experiments.

Introduction. Quantum droplet describes a self-bound many-body state that is stabilized by quantum effect. It has intrigued great attention recently in the field of ultracold atoms, given its successful observation in dipolar gases[1–7] and alkali Bose-Bose mixtures[8–11]. These dilute droplets, as pointed out in a pioneer work by Petrov[12], are stabilized by a subtle balance between the mean-field attraction and the Lee-Huang-Yang(LHY) repulsion from quantum fluctuations. Similar stabilization mechanism has been extended to other droplet systems including Bose-Fermi mixtures[13–18] and dipolar mixtures[19, 20].

The stability of quantum droplet depends crucially on the geometry. In three-dimension(3D), the quantum pressure can dissociate the droplet at small atom number and lead to the liquid-gas transition as observed in experiments[1–11]. In 2D and 1D, quantum droplet can be supported in quite different interaction regimes as compared to 3D, due to distinct LHY corrections[21]. In this context, it is conceptually important and also practically meaningful to investigate the confinement effect to droplet stability, which can bridge different droplet physics between different geometries. Previously, a few theoretical studies have revealed the significant change of LHY correction in quasi-low dimensions[22–25]. In particular, it has been shown that for alkali bosons the LHY energy can gradually change sign to negative as deepening the confinement[24, 25], while the resulted instability of droplet and its associated transitions during the dimensional reduction have not been discussed therein.

Apart from the significant change of LHY correction, the confinement will affect the droplet stability in two other non-trivial ways:

First, it introduces the boundary effect. As illustrated in Fig.1, for a droplet cloud confined uniformly with well-defined boundaries(central plot), the boundary ef-

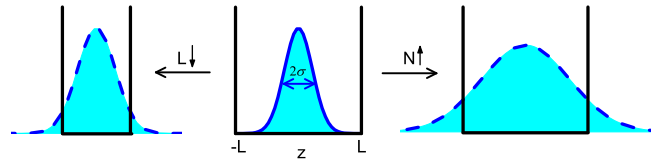


FIG. 1. Boundary effect to quantum droplet. Starting from a 3D droplet in a uniform trap with length much larger than the droplet size $L \gg \sigma$ (central plot), the boundary effect can become significant either by increasing the atom number (right) or by reducing the trap length (left). In both cases, we have $L \lesssim \sigma$ and the droplet will encounter instability. Here the droplet wave function is plotted only along the trap direction.

fect can become significant when the droplet size σ is comparable to the trap length L , either by increasing atom number N (right) or by reducing L (left). In either case, the droplet will adjust itself to be compatible with the boundary, which naturally causes instability. Second, the confinement can introduce another channel of bound state to compete with the droplet. A well known example is the bright soliton in quasi-1D(q1D) that is stabilized by quantum pressure and mean-field attraction[26–28]. In a recent experiment of Bose-Bose mixture[9], the droplet-soliton transition was explored in harmonically trapped quasi-1D, while the confinement effect to qualitative change of LHY correction was not considered.

In this work, by fully taking into account the confinement effect, we study the stability of quantum droplet and its associated transitions in Bose-Bose mixtures confined in q2D. To clearly see the boundary effect, we take the uniform confinement as depicted in Fig.1, which has become experimentally accessible with a tunable length[29–33]. We find that when the boundary effect becomes significant, as schematically shown in Fig.1, the

droplet will become unstable and give way to a soliton bound state that displays no density modulation along the confined direction. This leads to the reentrance of soliton ground state as increasing atom number, while the droplet can be stabilized only within certain number window that sensitively depends on the trap length. Near the droplet-soliton transitions, they can coexist with each other as two local minima in the energy landscape. Take the ^{39}K Bose-Bose mixture for example, we have analyzed in detail the competition physics between droplet and soliton and further mapped out the phase diagram for their transition and coexistence in terms of atom number and confinement length. These results can be readily tested in current cold atoms experiments.

Model. We consider the Hamiltonian for the Bose-Bose atomic mixture $H = \int d\mathbf{r}H(\mathbf{r})$ with: ($\hbar = 1$)

$$H(\mathbf{r}) = \sum_{i=1,2} \Psi_i^\dagger(\mathbf{r}) \left(-\frac{\nabla^2}{2m_i} \right) \Psi_i(\mathbf{r}) + \sum_{ij} \frac{g_{ij}}{2} \Psi_i^\dagger \Psi_j^\dagger \Psi_j \Psi_i(\mathbf{r}).$$

Here $\mathbf{r} = (x, y, z)$ is the coordinate; m_i and Ψ_i are respectively the mass and field operator of boson species i ; $g_{ii} = 4\pi a_{ii}/m_i$ and $g_{12} = 2\pi a_{12}/\mu$ ($\mu = m_1 m_2 / (m_1 + m_2)$) are the intra- and inter-species coupling constants. Given the atoms confined in a uniform trap with $z \in [-L, L]$ and under periodic boundary condition, the momentum along z are all quantized as $k_z = n\pi/L$, with $n = 0, \pm 1, \dots$. Based on the standard Bogoliubov theory for a homogeneous mixture with densities n_1, n_2 [34], we arrive at the following LHY energy per volume:

$$\mathcal{E}_{\text{LHY}} = \int \frac{d^2k}{2(2\pi)^2} \frac{1}{2L} \sum_n \left[E_{nk}^+ + E_{nk}^- - \sum_{i=1,2} (\epsilon_{nk}^{(i)} + g_{ii}n_i) \right] + \int \frac{d^3k}{2(2\pi)^3} \frac{m_1 g_{11}^2 n_1^2 + m_2 g_{22}^2 n_2^2 + 4\mu g_{12}^2 n_1 n_2}{k^2}, \quad (1)$$

where the quasi-particle energies read

$$E_{nk}^\pm = \sqrt{\frac{\omega_1^2 + \omega_2^2}{2} \pm \sqrt{\left(\frac{\omega_1^2 - \omega_2^2}{2}\right)^2 + 4g_{12}^2 n_1 n_2 \epsilon_{nk}^{(1)} \epsilon_{nk}^{(2)}}} \quad (2)$$

with $\omega_i = \sqrt{\epsilon_{nk}^{(i)}(\epsilon_{nk}^{(i)} + 2g_{ii}n_i)}$ and $\epsilon_{nk}^{(i)} = [(n\pi/L)^2 + k^2]/(2m_i)$. We note that the LHY energy in quasi-low D was studied previously with different techniques aiming at the equal-mass mixtures[24, 25]. In comparison, here our scheme applies for an arbitrary mass ratio m_1/m_2 .

To investigate the instability of self-bound state, we have to go beyond the bulk description and employ a spatially varying wave function $\Psi_i(\mathbf{r})$. By assuming an identical spatial mode for both species $\Psi_i(\mathbf{r}) = \sqrt{N_i}\phi(\mathbf{r})$, we arrive at the energy functional

$$E = E_{\text{kin}} + E_{\text{mf}} + E_{\text{LHY}}, \quad (3)$$

with $E_{\text{kin}} = \sum_i N_i \int d\mathbf{r} \phi^*(\mathbf{r}) \left(-\frac{\nabla^2}{2m_i} \right) \phi(\mathbf{r})$, $E_{\text{mf}} = (g_{11}N_1^2/2 + g_{22}N_2^2/2 + g_{12}N_1N_2) \int d\mathbf{r} |\phi(\mathbf{r})|^4$ and $E_{\text{LHY}} =$

$\int d\mathbf{r} \mathcal{E}_{\text{LHY}}(n_i(\mathbf{r}))$, where $n_i(\mathbf{r}) = N_i |\phi_i(\mathbf{r})|^2$. We also assume the number ratio as $N_1/N_2 = \sqrt{g_{22}/g_{11}}$ in order to minimize E_{mf} [12]. Above assumptions have been shown to well predict the liquid-gas transition in 3D droplets[8]. For the current case with a uniform trap and periodic boundary condition $\phi(\mathbf{r}) = \phi(\mathbf{r} + 2L\mathbf{e}_z)$, we adopt the following Gaussian-type variational ansatz :

$$\phi(\mathbf{r}) = \frac{1}{\sqrt{\mathcal{N}}} \exp\left(-\frac{x^2 + y^2}{2\sigma_{xy}^2}\right) \left[\sum_{\nu=-\infty}^{\infty} \exp\left(-\frac{(z - 2\nu L)^2}{2\sigma_z^2}\right) \right]. \quad (4)$$

Here \mathcal{N} is the normalization factor; σ_{xy} and σ_z are two variational parameters and represent, respectively, the sizes of bound state along xy and z directions. The ground state can be obtained by minimizing the energy functional (3) in terms of σ_{xy} and σ_z .

In this work, we specifically consider the two hyperfine states of ^{39}K atoms, $|1\rangle \equiv |F=1, m_F=0\rangle$, $|2\rangle \equiv |F=1, m_F=-1\rangle$, as have been well studied in 3D droplet experiments[8–10]. In this case, $a_{22} = 35a_B$, $a_{12} = -53a_B$ (a_B is the Bohr radius), and a_{11} is highly tunable by magnetic field. We will focus on the mean-field collapse regime with $\delta a \equiv a_{12} + \sqrt{a_{11}a_{22}} < 0$ and study how the uniform confinement affects the quantum droplet. As we consider small $|\delta a| (\ll a_{11}, a_{22}, |a_{12}|)$, in calculating E_{LHY} we make the approximation $\delta a = 0$ to avoid the photon instability due to complex spectrum (2). Other rectified theories on this have appeared recently[35–37]. Throughout the paper, we choose the length unit as $l_0 = 1\mu\text{m}$ and the energy unit as $E_0 = 1/(2ml_0^2)$, with mass $m \equiv m_1 = m_2$ for ^{39}K atoms.

Results. By searching for the energy minimum in terms of σ_{xy} and σ_z , i.e., $\partial E/\partial\sigma_{xy,z} = 0$ and $\partial^2 E/\partial\sigma_{xy,z}^2 > 0$, we find two candidates for the ground state: a droplet state if both σ_{xy} and σ_z are finite, and a soliton state if σ_{xy} is finite and $\sigma_z \rightarrow \infty$ (no density modulation along z). Different from free space case, here no gaseous ground state (both $\sigma_{xy,z} \rightarrow \infty$) can be found when L is finite.

(I) *Droplet solution.* Fig.2 shows the droplet solution as varying N at several typical L . One can see from Fig.2(a) that the droplet energy continuously decreases as shrinking L , which can be attributed to the reduced kinetic and LHY energies. Moreover, another remarkable effect of finite L is that, now the droplet only survives within a finite number window $[N_{d1}, N_{d2}]$, unlike the free space droplet that just requires a lower number bound. This number window becomes narrower for smaller L , due to the existence of another competitive channel of bound state (soliton, as discussed later). In particular, we see that a small L also gives rise to a small upper bound N_{d2} , and this is consistent with the boundary effect as illustrated in Fig.1.

Fig.2(b1,b2) show that the droplet sizes σ_{xy} and σ_z both evolve non-monotonically with N . Near the vanishing point of droplet ($N \sim N_{d2}$), shrinking L will lead to a smaller σ_{xy} but a larger σ_z . This means that by tight-

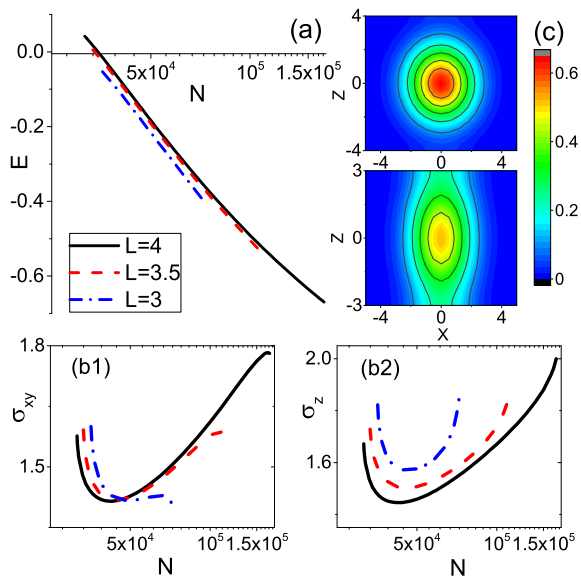


FIG. 2. Droplet state of ^{39}K atoms in q2D with $\delta a = -5a_B$. (a) Droplet energy E as a function of atom number N at different $L = 4, 3.5, 3$. (b1,b2) Droplet sizes σ_{xy} and σ_z as functions of N at various L . (c) Contour plot of droplet wave function $\phi(\mathbf{r})$ in (x,z) plane (with $y = 0$) for a given $N = 7 \times 10^4$ at $L = 4$ (upper panel) and 3 (lower panel). Here the length and energy units are respectively $l_0 = 1\mu\text{m}$ and $E_0 = 1/(2ml_0^2)$.

ening the confinement, more weight of the droplet transfers from the free (xy) to confined (z) direction; accordingly, its wave function will change from a nearly isotropic shape (3D case) to a highly elongated one (more extended along z), as shown in Fig.2(c). This counter-intuitive change can be understood as follows: a tight confinement (small L) can induce a large energy gap along z , and therefore the system tends to minimize the density modulation in this direction to suppress E_{kin} , which leads to a more extended wave function along z .

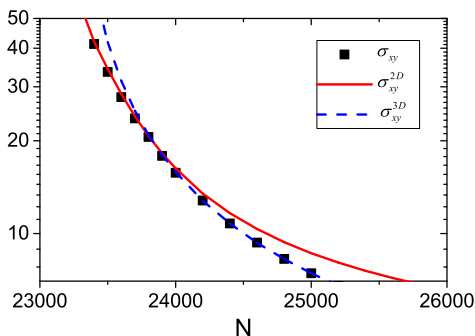


FIG. 3. Transverse size of soliton state, σ_{xy} (black square), for ^{39}K atoms in q2D. Here $\delta a = -5a_B$ and $L = 3$. Red solid and blue dashed lines show function fit to Eqs.(5) and (6). The length unit is $l_0 = 1\mu\text{m}$.

(II) *Soliton solution.* The uniform trap along z can also support another type of bound state ($E < 0$) at $\sigma_z = \infty$ and a finite σ_{xy} , where the density modulation is allowed only along the free (xy) directions and we refer to this type of bound state as soliton. Different from the q1D soliton[26–28], here only the kinetic and mean-field terms are inadequate to support the q2D soliton. For instance, in the 2D limit we have $E_{\text{kin}} \sim \sigma_{xy}^{-2}$ and $E_{\text{kin}} \sim -L^{-1}\sigma_{xy}^{-2}$, and one has to incorporate the contribution from E_{LHY} to stabilize the energy minimum at finite σ_{xy} . It is noted that such LHY-stabilized soliton in 2D limit is equivalent to the 2D droplet considered in Ref.[21].

Combining Eqs.(3,4) with the analytical expressions of ϵ_{LHY} for an equal-mass homogeneous mixture at low density (2D limit) or high density(3D limit)[24], we obtain the equilibrium size of soliton in both limits as:

$$\sigma_{xy}^{2\text{D}} = 4LD^{1/2}\exp\left(\frac{1}{2} - \frac{NC}{4D^2}\right), \quad (5)$$

$$\sigma_{xy}^{3\text{D}} = \frac{1024L}{25\pi} \frac{D^{5/2}}{NC}, \quad (6)$$

with $C = -1 - 2N_1N_2\delta a/(NL)$ and $D = (N_1a_{11} + N_2a_{22})/(2L)$. In Fig.3 we show the soliton size σ_{xy} as varying N at fixed $L = 3\mu\text{m}$, and we see that Eqs.(5,6) fit well to σ_{xy} respectively in small and large N limit.

(III) *Droplet-soliton transition and coexistence.* After identifying the individual property of droplet and soliton, now we turn to investigate their competition. In Fig.4, we demonstrate their transition and coexistence as tuning N for a fixed $L = 3.5\mu\text{m}$. As seen from Fig.4(a), the energies of droplet and soliton cross twice as increasing N , which determine two transition points respectively at N_{c1} and N_{c2} . Their individual stability and mutual competition can be clearly seen from the energy contour plots $E(\sigma_{xy}, \sigma_z)$ in Fig.4(c1-c5), together with the comparison of their transverse sizes σ_{xy} shown in Fig.4(b).

For small N , the only energy minimum represents a soliton state, i.e., at $\sigma_z \rightarrow \infty$ and a finite σ_{xy} (see Fig.4(c1)). As increasing N to N_{d1} , the droplet start to emerge as an additional energy minimum at finite σ_z and a smaller σ_{xy} (see Fig.4(b)). The double minima reach the same energy when tune N to the first transition point N_{c1} (see Fig.4(c2)).

To facilitate the discussion, let us define the *droplet region* in the energy landscape along σ_{xy} , with lower bound $\sigma_{xy}^{d,low}$ and upper bound $\sigma_{xy}^{d,upp}$ (marked by the dashed-dot and dashed lines in Fig.4(c2-c4)). Within this region, i.e., for any $\sigma_{xy} \in (\sigma_{xy}^{d,low}, \sigma_{xy}^{d,upp})$, the energy minimum occurs at a finite σ_z . Once the soliton enters this region, i.e., when its size $\sigma_{xy}^s \in (\sigma_{xy}^{d,low}, \sigma_{xy}^{d,upp})$, the soliton will become unstable and flow from $\sigma_z = \infty$ to the droplet minimum. In Fig.4(b), we denote the atom number at the intersection of σ_{xy}^s and $\sigma_{xy}^{d,upp}$ ($\sigma_{xy}^{d,low}$) as N_{s1} (N_{s2}). Correspondingly, when $N \in [N_{s1}, N_{s2}]$ the soliton becomes locally unstable and the droplet is the only stable (ground) state, see Fig.4(c3). For N beyond N_{s2} , the soli-

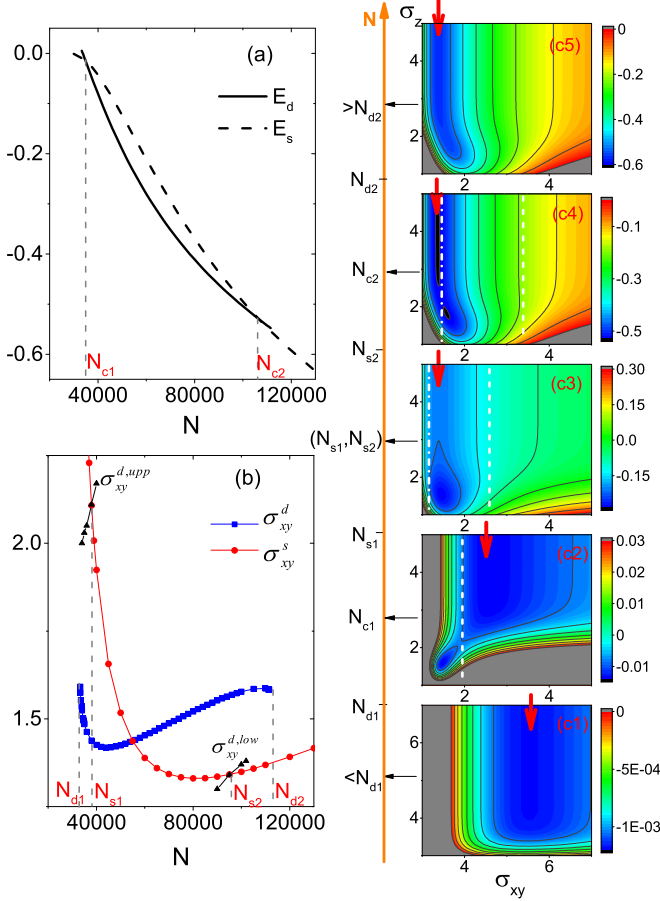


FIG. 4. Droplet-Soliton transition and coexistence at $\delta a = -5a_B$ and $L = 3.5\mu m$. (a) Energies of droplet (E_d) and soliton (E_s) as functions of N . The energy crossings determine two transition points at N_{c1} and N_{c2} . (b) Transverse sizes of droplet (σ_{xy}^d) and soliton (σ_{xy}^s), in comparison with $\sigma_{xy}^{d,low}$ and $\sigma_{xy}^{d,upp}$ defining the droplet region (see text). The droplet is locally stable for $N \in (N_{d1}, N_{d2})$, and is the only stable (ground) state for $N \in (N_{s1}, N_{s2})$ when the soliton enters droplet region. Droplet-soliton coexistence occurs at $N \in (N_{d1}, N_{s1}) \cup (N_{s2}, N_{d2})$. (c1-c5) Contour plot of $E(\sigma_{xy}, \sigma_z)$ for various $N(10^4)$: 3(c1), 3.48(= N_{c1} , c2), 6(c3), 10.66(= N_{c2} , c4), 11.5(c5). The white dashed-dot and dashed lines mark the locations of $\sigma_{xy}^{d,low}$ and $\sigma_{xy}^{d,upp}$, and the red arrows mark σ_{xy}^s . The length and energy units are the same as Fig.2.

ton moves outside the droplet region and they can again coexist. Their second transition occurs at N_{c2} when the two minima have the same energy, see Fig.4(c4). The coexistence stops at $N = N_{d2}$ when the droplet solution disappears, and for $N > N_{d2}$ the only ground state becomes soliton again, see Fig.4(c5).

From above, we can see that the droplet-soliton competition is most pronounced when the soliton enters the droplet region, or equivalently, when they have similar sizes along free (xy) directions. On the other hand, at large atom number ($N > N_{d2}$) the instability of droplet

as well as the reentrance of soliton is mostly caused by the boundary effect(see Fig.1), when the droplet size along the confined (z) direction is comparable with the trap length. For instance, at N_{d2} the droplet size reaches $\sigma_z = 1.86\mu m$, beyond half of trap length $L = 3.5\mu m$.

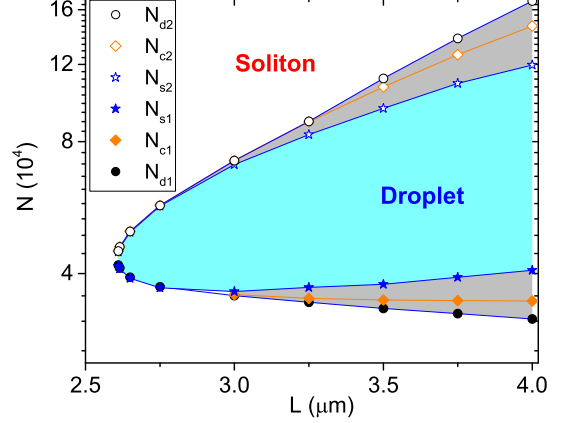


FIG. 5. Phase diagram in the (N, L) plane for ^{39}K mixture at $\delta a = -5a_B$. The droplet, soliton, and their coexistence regions are respectively shown by blue, white, and gray colors. Their phase boundaries are given by N_{d1} , N_{s1} , N_{s2} and N_{d2} (see text). Droplet-soliton transitions (energy crossing) occur at N_{c1} and N_{c2} , denoted by solid and hollow orange diamonds.

(IV) Phase diagram. To fully explore the confinement effect, we have carried out similar analysis for different L and arrived at the phase diagram in the (N, L) plane as shown in Fig.5. One can see that the droplet state (blue color) only survives within a finite number window that sensitively depends on the value of L . It will give way to the soliton state (white color) for very large or small N , or for small L . Near their transition points N_{c1} and N_{c2} (orange diamonds), the droplet and soliton can coexist with each other, and their coexistence region (gray color) also depends sensitively on L .

In fact, for $L \in (2.6, 3)\mu m$ we find continuous transitions between droplet and soliton, i.e., the location of energy minimum continuously change between finite and infinite σ_z across the phase boundaries; for $L < 2.6\mu m$, no droplet solution can be found and the soliton is the only stable (ground) state. A physical picture for this finding is that, for very small L , the large energy gap along z rules out the possibility of density modulation in this direction, and thus the soliton state is always more favored for any particle number.

Fig.5 can be readily detected in experiments. The droplet and soliton states can be identified by measuring their density modulations along the confined direction, and their transitions can be explored through the discontinuous number change or droplet fragmentation when sweeping across the phase boundary, as recently conducted in experiment with a different setup[9].

Discussion. In this work we have adopted the local density approximation(LDA) to compute E_{LHY} , which was shown to predict the transitions in 3D droplets quantitatively well[8, 10]. Here we remark that the LDA is even more qualified in our case, especially along the confined direction with small L . This is because as reducing L , the droplet density gets more elongated along z (see Fig.2(c)) and the kinetic energy is further suppressed. In fact, we have checked that $\eta_z \equiv E_{\text{kin},z}/E_{\text{LHY}} \ll 1$ is satisfied in a broad parameter regime we considered. Take the case in Fig.4 for instance, the ratio η_z is 0.46 at N_{c1} and gets even smaller to 0.08 at N_{c2} . This is to say, the typical length at which the density varies is visibly longer than that characterizing the LHY correction, which justifies the application of LDA in our setup.

Finally, it is worth to point out that the boundary effect revealed here is unlikely to apply for harmonic confinements, where the boundary cannot be clearly defined and the eigen-mode is also different. This follows that the physics near N_{c2} , as mostly driven by the boundary effect, would disappear for harmonically confined systems. This expectation is consistent with the recent experimental study of harmonically trapped Bose-Bose mixtures in q1D, where only one droplet-soliton transition (corresponding to N_{c1} in this work) was observed[9].

Acknowledgment. The work is supported by the National Key Research and Development Program of China (2018YFA0307600, 2016YFA0300603), the National Natural Science Foundation of China (No.11534014, No.12074419), and the Strategic Priority Research Program of Chinese Academy of Sciences (No. XDB33000000).

* xlcul@iphy.ac.cn

- [1] I. Ferrier-Barbut, H. Kadau, M. Schmitt, M. Wenzel, and T. Pfau, Phys. Rev. Lett. **116**, 215301 (2016).
- [2] M. Schmitt, M. Wenzel, F. Böttcher, I. Ferrier-Barbut, and T. Pfau, Nature **539**, 259 (2016).
- [3] I. Ferrier-Barbut, M. Schmitt, M. Wenzel, H. Kadau, and T. Pfau, J. Phys. B **49**, 214004 (2016).
- [4] L. Chomaz, S. Baier, D. Petter, M.J. Mark, F. Wächtler, L. Santos, and F. Ferlaino, Phys. Rev. X **6**, 041039 (2016).
- [5] L. Tanzi, E. Lucioni, F. Famà, J. Catani, A. Fioretti, C. Gabbanini, R. N. Bisset, L. Santos, and G. Modugno, Phys. Rev. Lett. **122**, 130405 (2019).
- [6] F. Böttcher, J.-N. Schmidt, M. Wenzel, J. Hertkorn, M. Guo, T. Langen, and T. Pfau, Phys. Rev. X **9**, 011051 (2019).
- [7] L. Chomaz, D. Petter, P. Ilzhöfer, G. Natale, A. Trautmann, C. Politi, G. Durastante, R.M.W. van Bijnen, A. Patscheider, M. Sohmen, M.J. Mark, and F. Ferlaino, Phys. Rev. X **9**, 021012 (2019).
- [8] C.R. Cabrera, L. Tanzi, J. Sanz, B. Naylor, P. Thomas, P. Cheiney, and L. Tarruell, Science **359**, 301 (2018).
- [9] P. Cheiney, C. R. Cabrera, J. Sanz, B. Naylor, L. Tanzi, L. Tarruell, Phys. Rev. Lett. **120**, 135301 (2018).
- [10] G. Semeghini, G. Ferioli, L. Masi, C. Mazzinghi, L. Wolswijk, F. Minardi, M. Modugno, G. Modugno, M. Inguscio, M. Fattori, Phys. Rev. Lett. **120**, 235301 (2018).
- [11] C. D’Errico, A. Burchianti, M. Prevedelli, L. Salasnich, F. Ancilotto, M. Modugno, F. Minardi, and C. Fort, Phys. Rev. Research **1**, 033155 (2019).
- [12] D.S. Petrov, Phys. Rev. Lett. **115**, 155302 (2015).
- [13] X. Cui, Phys. Rev. A **98**, 023630 (2018).
- [14] S. Adhikari, Laser Phys. Lett **15**, 095501 (2018).
- [15] D. Rakshit, T. Karpiuk, M. Brewczyk, and M. Gajda, SciPost Phys **6**, 079 (2019).
- [16] D. Rakshit, T. Karpiuk, P. Zin, M. Brewczyk, M. Lewenstein, and M. Gajda, New J. Phys. **21**, 073027 (2019).
- [17] M. Wenzel, T. Pfau and I. Ferrier-Barbut, Physica Scripta **93**, 10 (2018).
- [18] J.-B. Wang, J.-S. Pan, X. Cui, W. Yi, Chin. Phys. Lett. **37**, 076701 (2020).
- [19] Joseph C. Smith, D. Baillie, and P. B. Blakie, arxiv:2007.00366.
- [20] R. N. Bisset, L. A. Peña Ardila, and L. Santos, arxiv:2007.00404.
- [21] D. S. Petrov and G. Astrakharchik, Phys. Rev. Lett. **117**, 100401 (2016).
- [22] D. Edler, C. Mishra, F. Wächtler, R. Nath, S. Sinha, and L. Santos, Phys. Rev. Lett. **119**, 050403 (2017).
- [23] K. Jachymski and R. Oldziejewski, Phys. Rev. A **98**, 043601 (2018).
- [24] P. Zin, M. Pylak, T. Wasak, M. Gajda, and Z. Idziaszek, Phys. Rev. A **98**, 051603(R) (2018).
- [25] T. Ilg, J. Kuhlmann, L. Santos, D. S. Petrov, and H. P. Büchler, Phys. Rev. A **98**, 051603(R) (2018).
- [26] V. M. Pérez-García, H. Michinel, and H. Herrero, Phys. Rev. A **57**, 3837 (1998).
- [27] K. E. Strecker, G. B. Partridge, A. G. Truscott, and R. G. Hulet, Nature **417**, 150 (2002).
- [28] L. Khaykovich, F. Schreck, G. Ferrari, T. Bourdel, J. Cubizolles, L. D. Carr, Y. Castin, and C. Salomon, Science **296**, 1290 (2002).
- [29] A. L. Gaunt, T. F. Schmidutz, I. Gotlibovych, R. P. Smith, and Z. Hadzibabic, Phys. Rev. Lett. **110**, 200406 (2013).
- [30] I. Gotlibovych, T. F. Schmidutz, A. L. Gaunt, N. Navon, R. P. Smith, Z. Hadzibabic, Phys. Rev. A **89**, 061604(R) (2014).
- [31] C. Eigen, A. L. Gaunt, A. Suleymanzade, N. Navon, Z. Hadzibabic, R. P. Smith, Phys. Rev. X **6**, 041058 (2016).
- [32] B. Mukherjee, Z. Yan, P. B. Patel, Z. Hadzibabic, T. Yefsah, J. Struck, and M. W. Zwierlein, Phys. Rev. Lett. **118**, 123401 (2018).
- [33] K. Hueck, N. Luick, L. Sobirey, J. Siegl, T. Lompe, and H. Moritz, Phys. Rev. Lett. **120**, 060402 (2018).
- [34] C. J. Pethick and H. Smith, *Bose-Einstein Condensation in Dilute Gases*, Cambridge University Press, 2002.
- [35] H. Hu and X.-J. Liu, arXiv:2005.08581.
- [36] M. Ota and G. E. Astrakharchik, SciPost Phys. **9**, 020 (2020).
- [37] Q. Gu, L. Yin, arxiv:2005.13154.